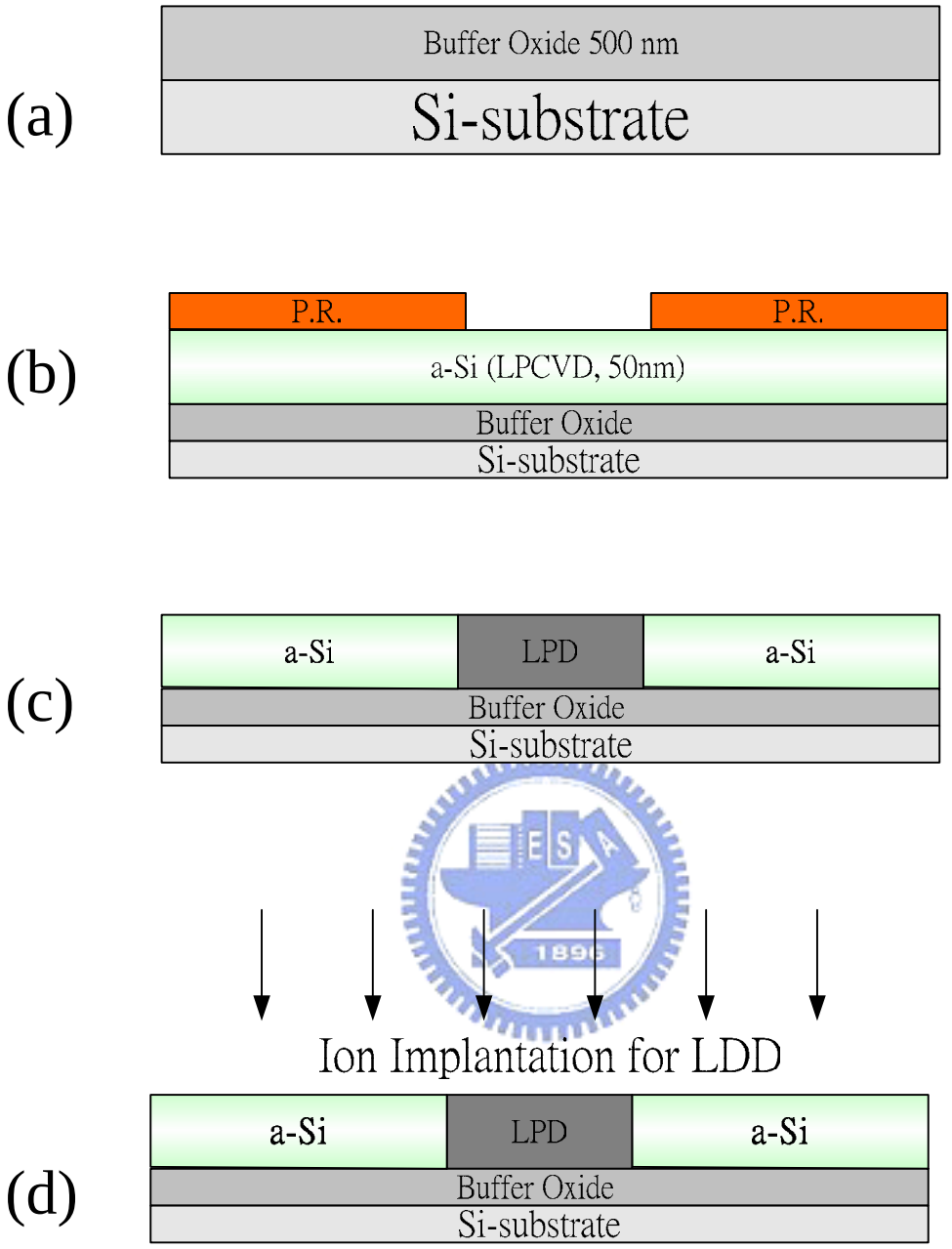

Figure 2-1 Process flow of ECTFT sample with GOLDD structure

(e)

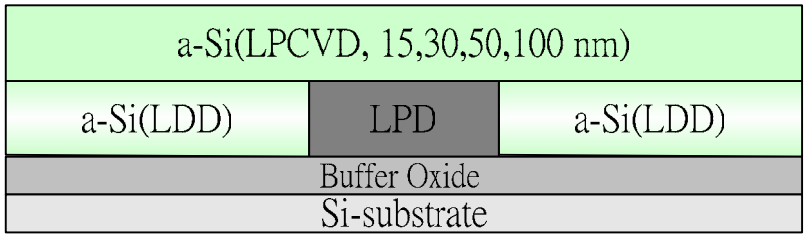

(f)

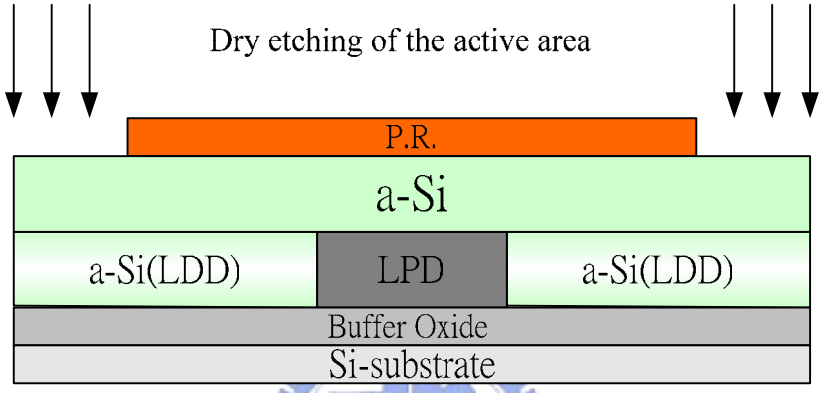

(g)

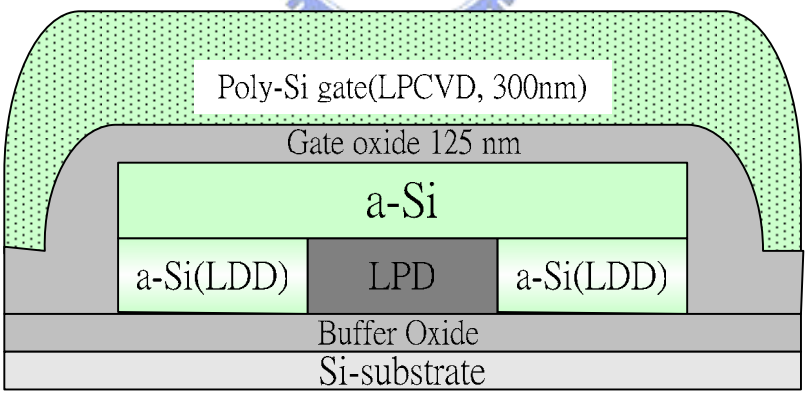

Figure 2-1 Process flow of ECTFT sample with GOLDD structure

(h)

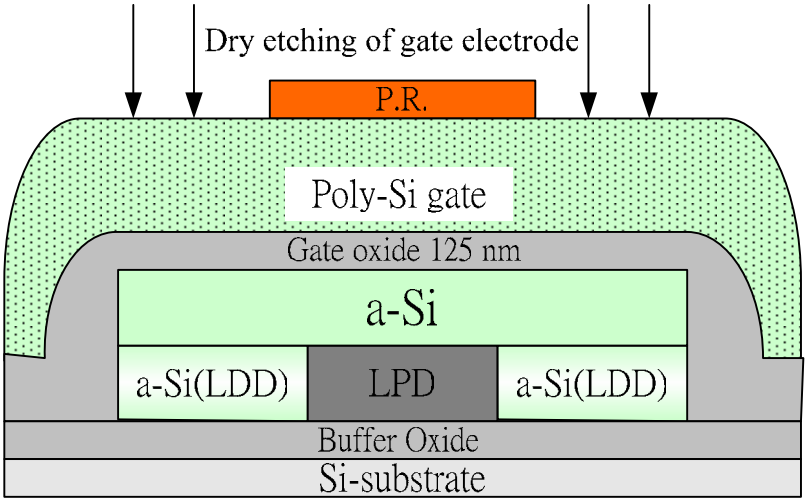

(i)

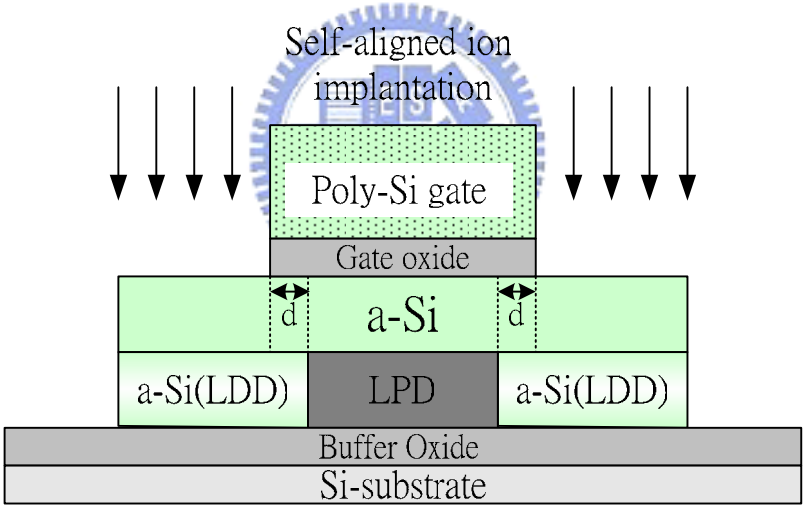

Figure 2-1 Process flow of ECTFT sample with GOLDD structure

(j)

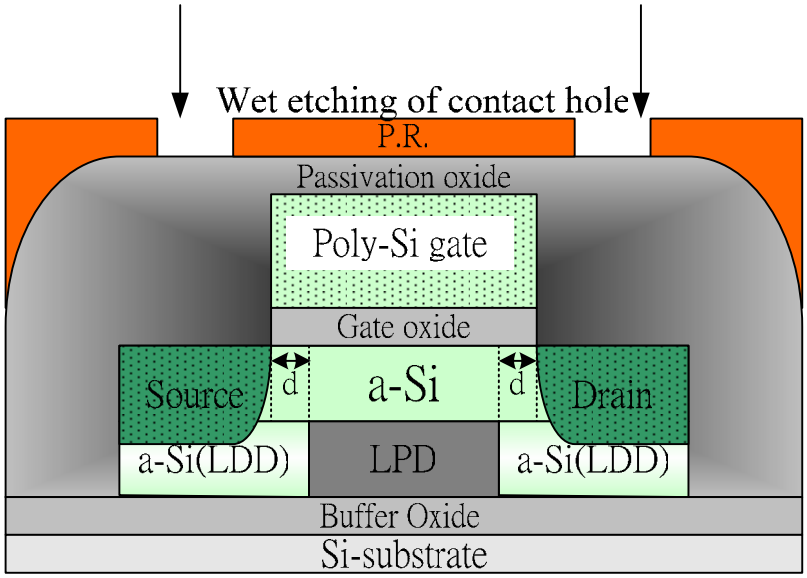

(k)

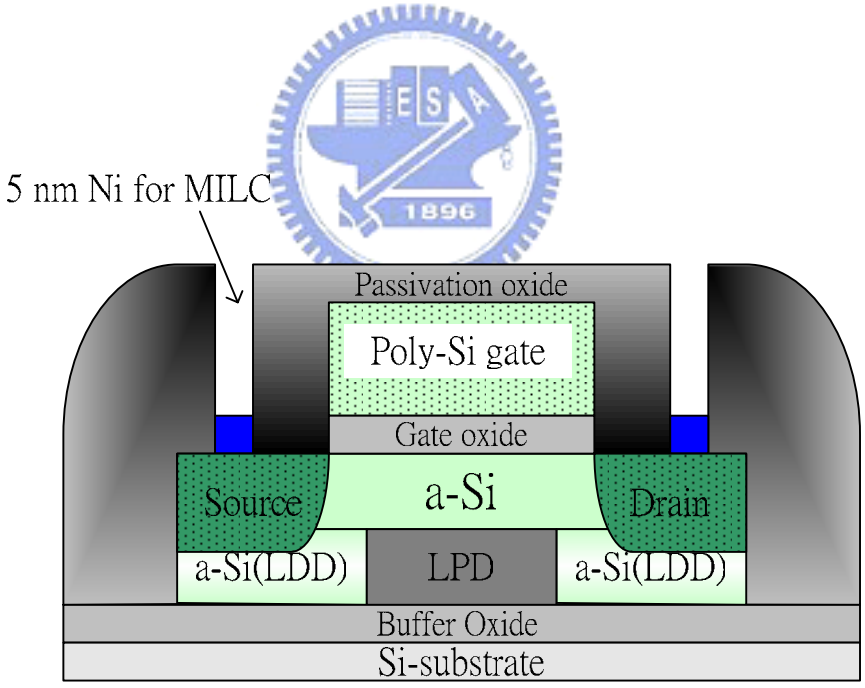

Figure 2-1 Process flow of ECTFT sample with GOLDD structure

(l)

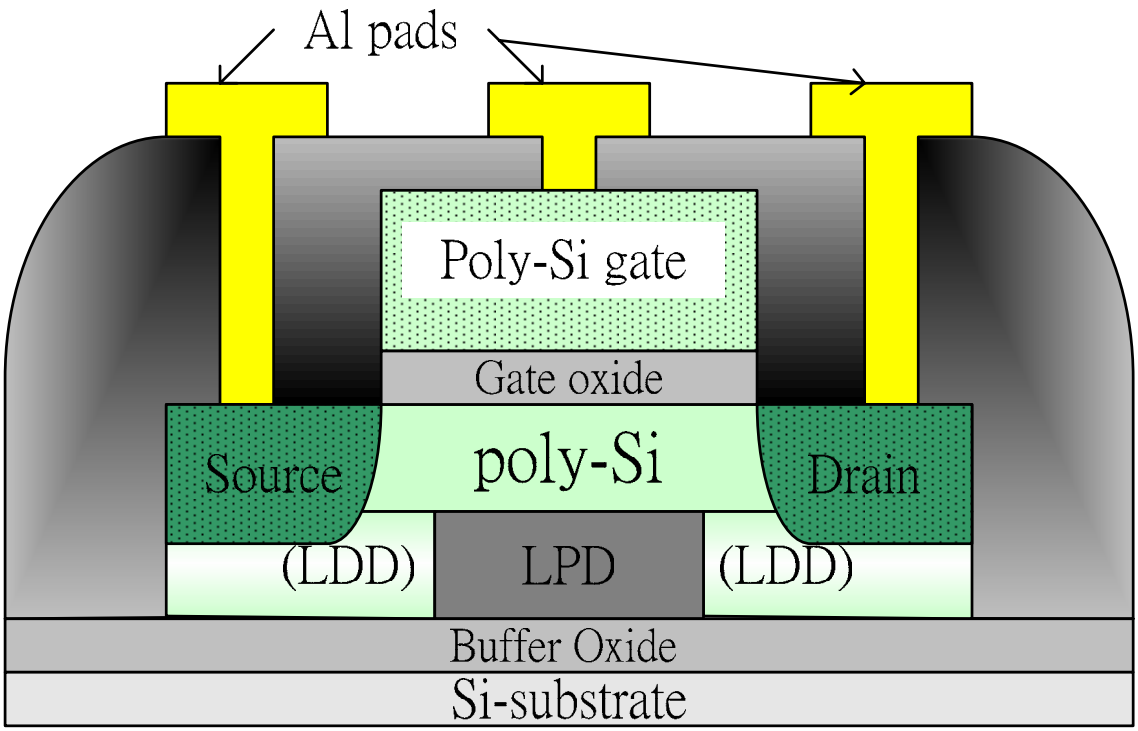

Figure2-1 Process flow of ECTFT sample with GOLDD structure

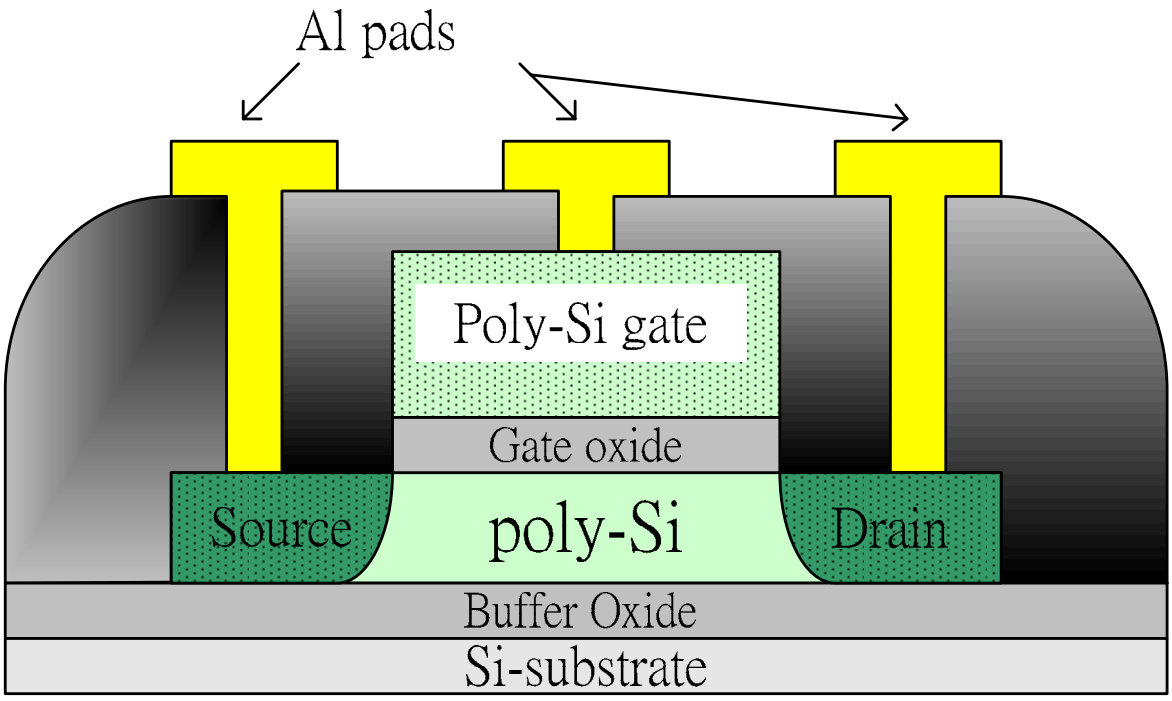

Figure 2-2 Cross-sectional view of a conventional top-gate TFT

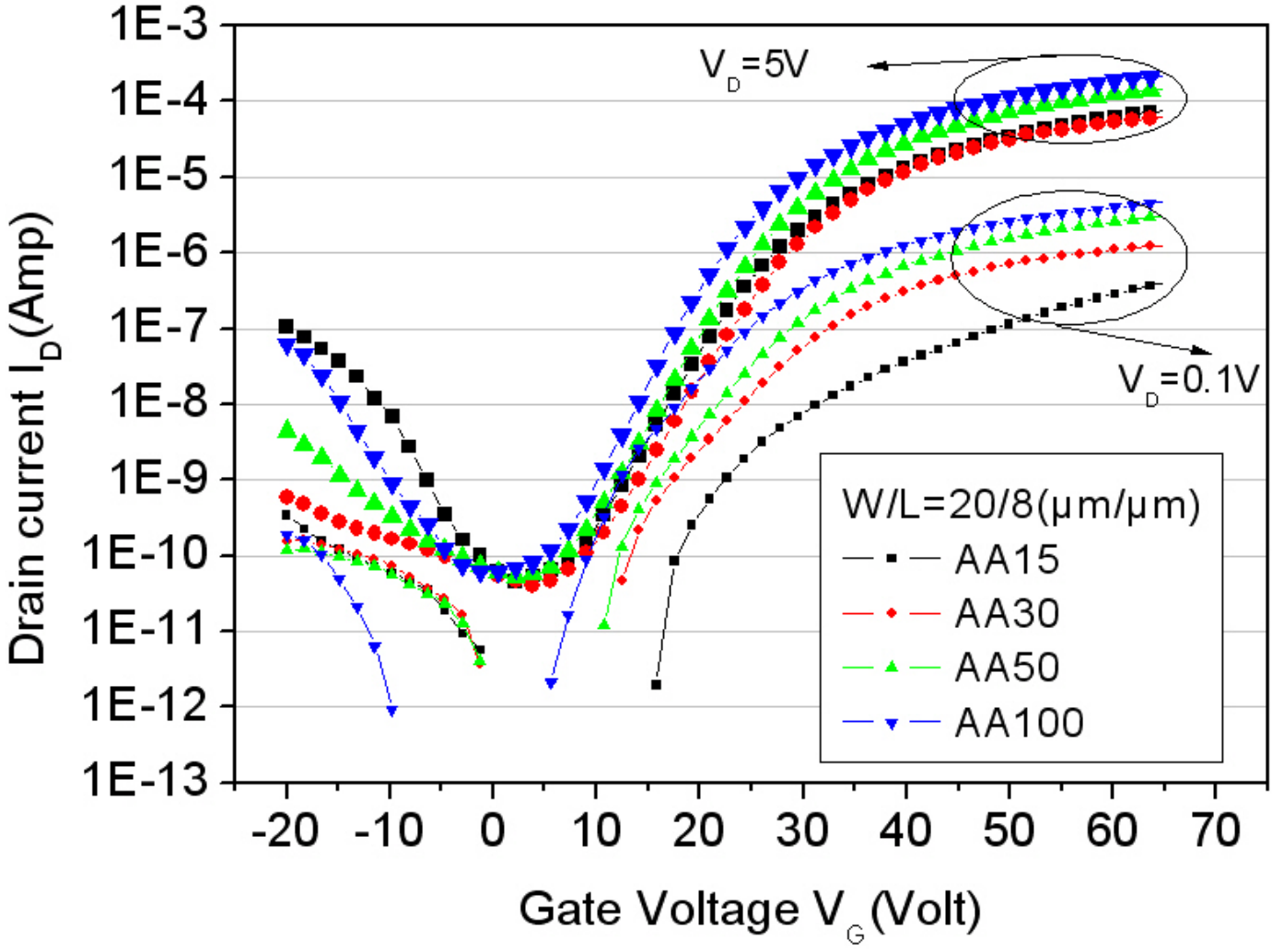

Figure 2-3 I_D - V_{GS} curves of conventional TFTs with different thickness of the active layer

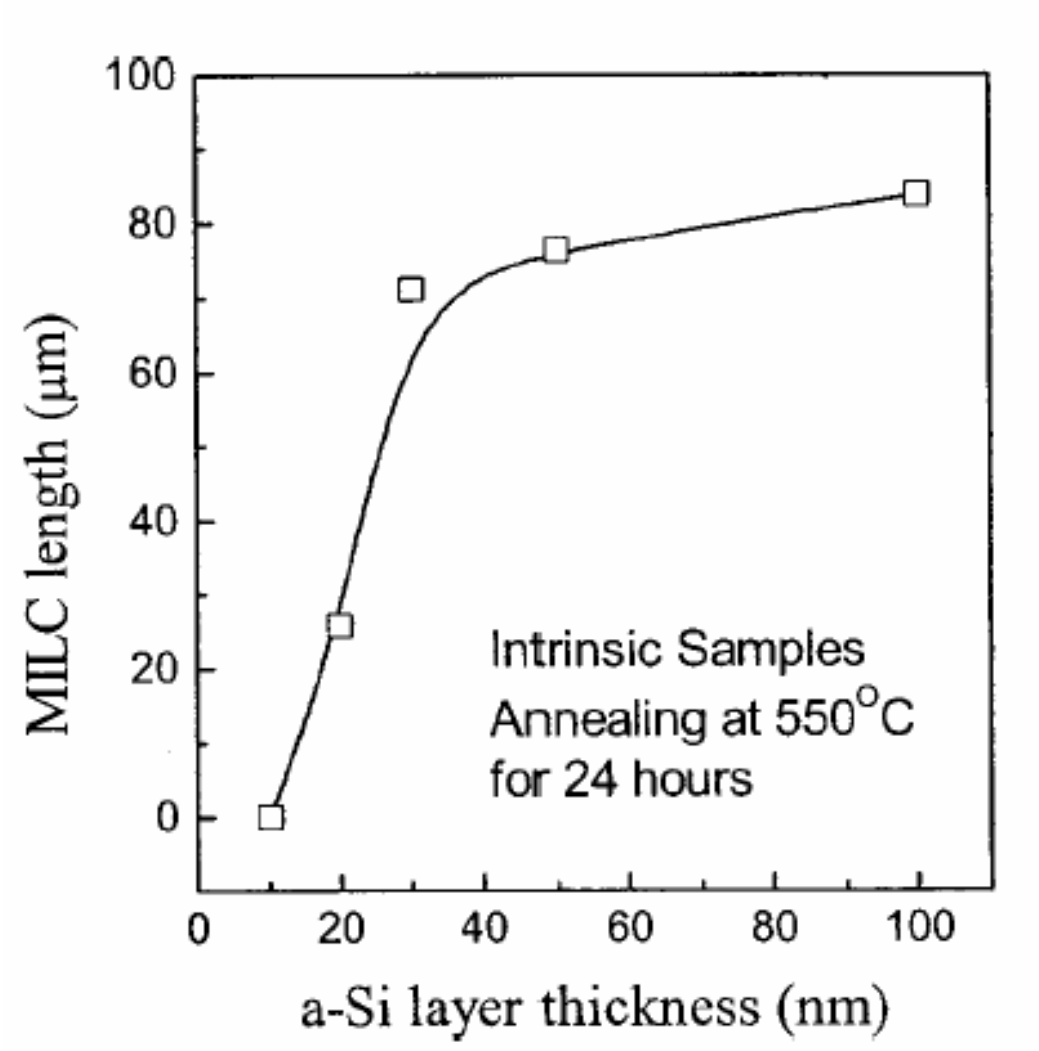

Figure 2-4 The dependence of MILC length on a-Si layer thickness after heat treatment 550℃ for 24 hr [ref. 2.13].

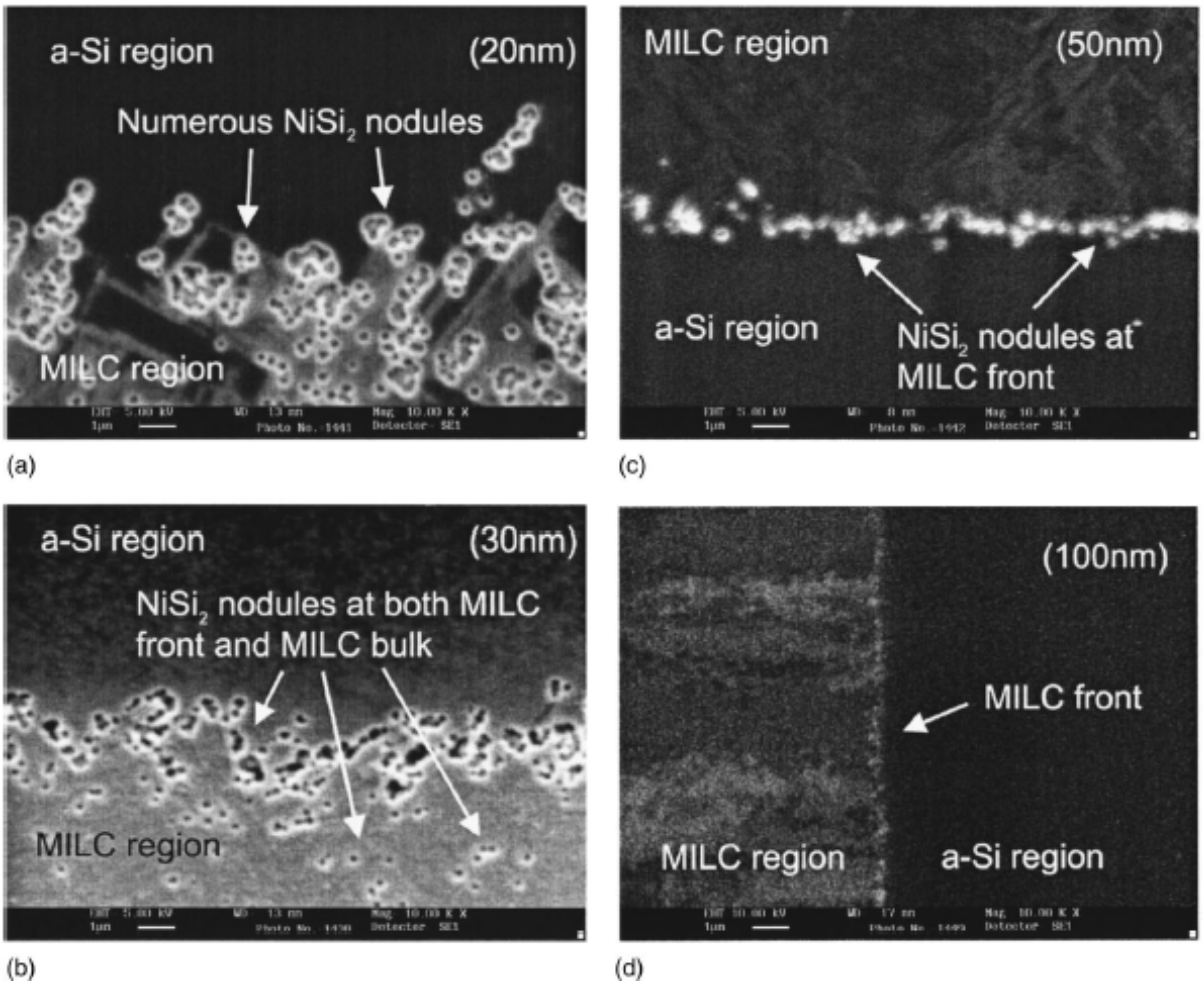

Figure 2-5 SEM micrographs of MILC front regions with different a-Si layer thickness : (a) 20, (b) 30, (c) 50, (d) 100 nm.[ref. 2.13]

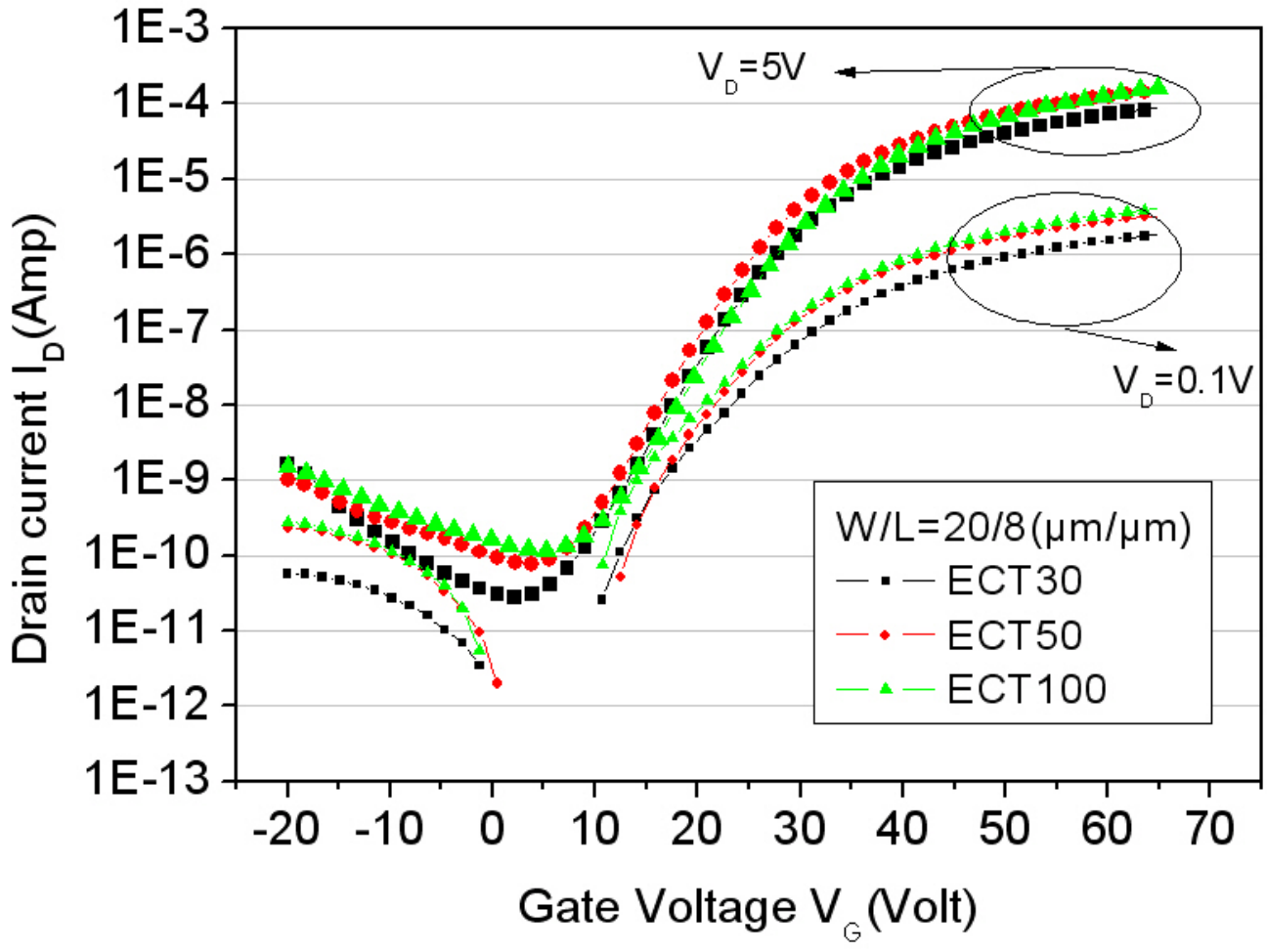

Figure 2-6 Transfer curves of ECTFT structure (d=0, d : gate overlapping length) with different thickness of the active layer

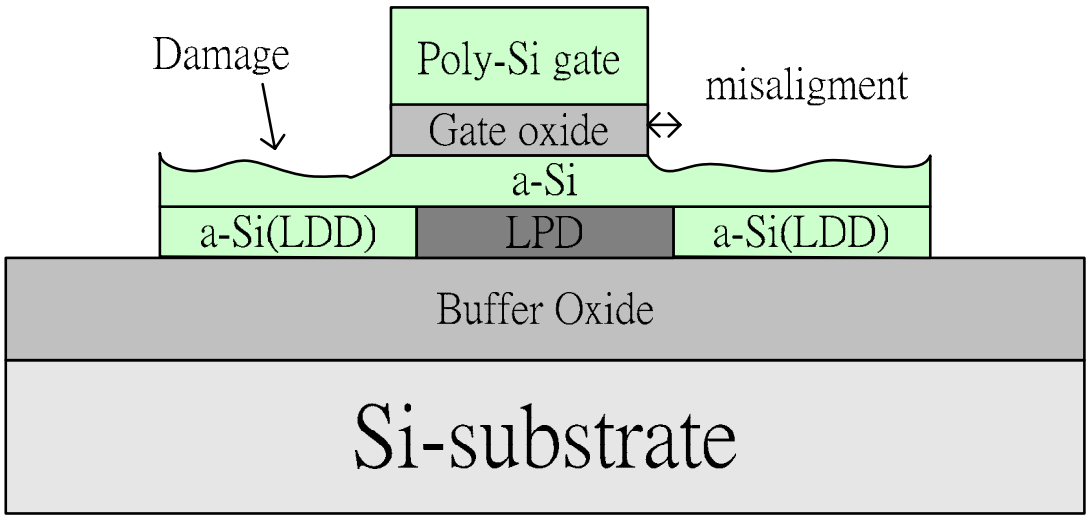

(A)

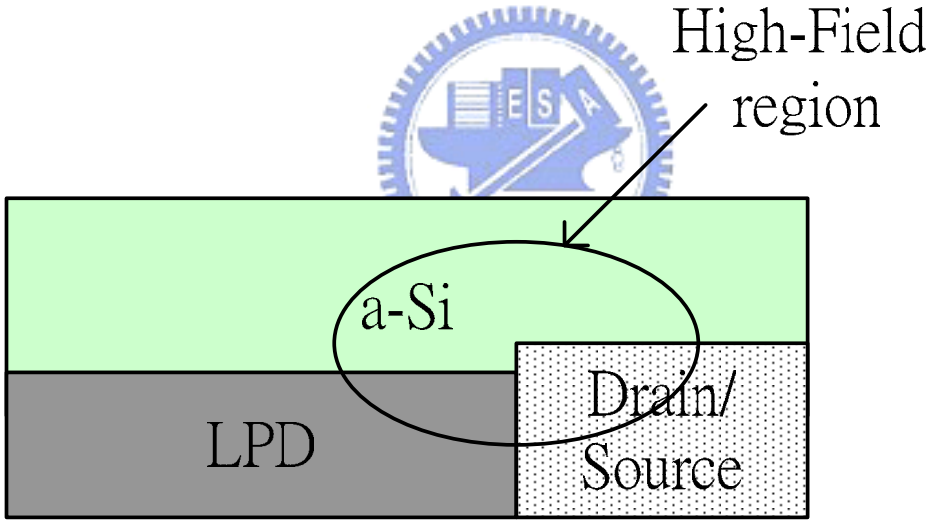

(B)

Figure 2-7 Failure mechanism of sample ECT15: (a) misalignment of top gate electrodes and channel over etching, and (b) planarization of LPD with large electric field at the trench corner

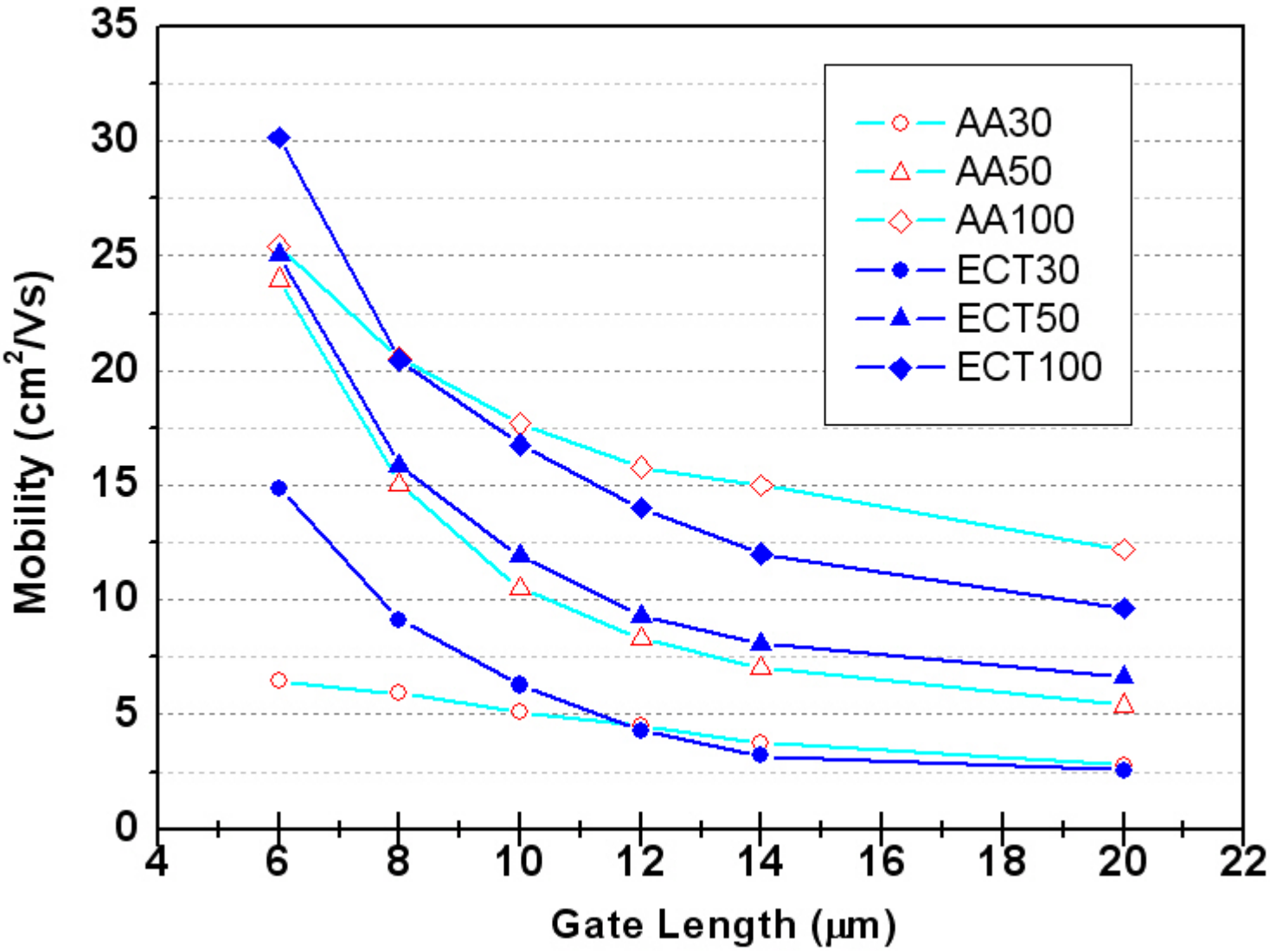

Figure 2-8 The field-effect mobility versus gate length for TFTs with different channel thickness and device structure

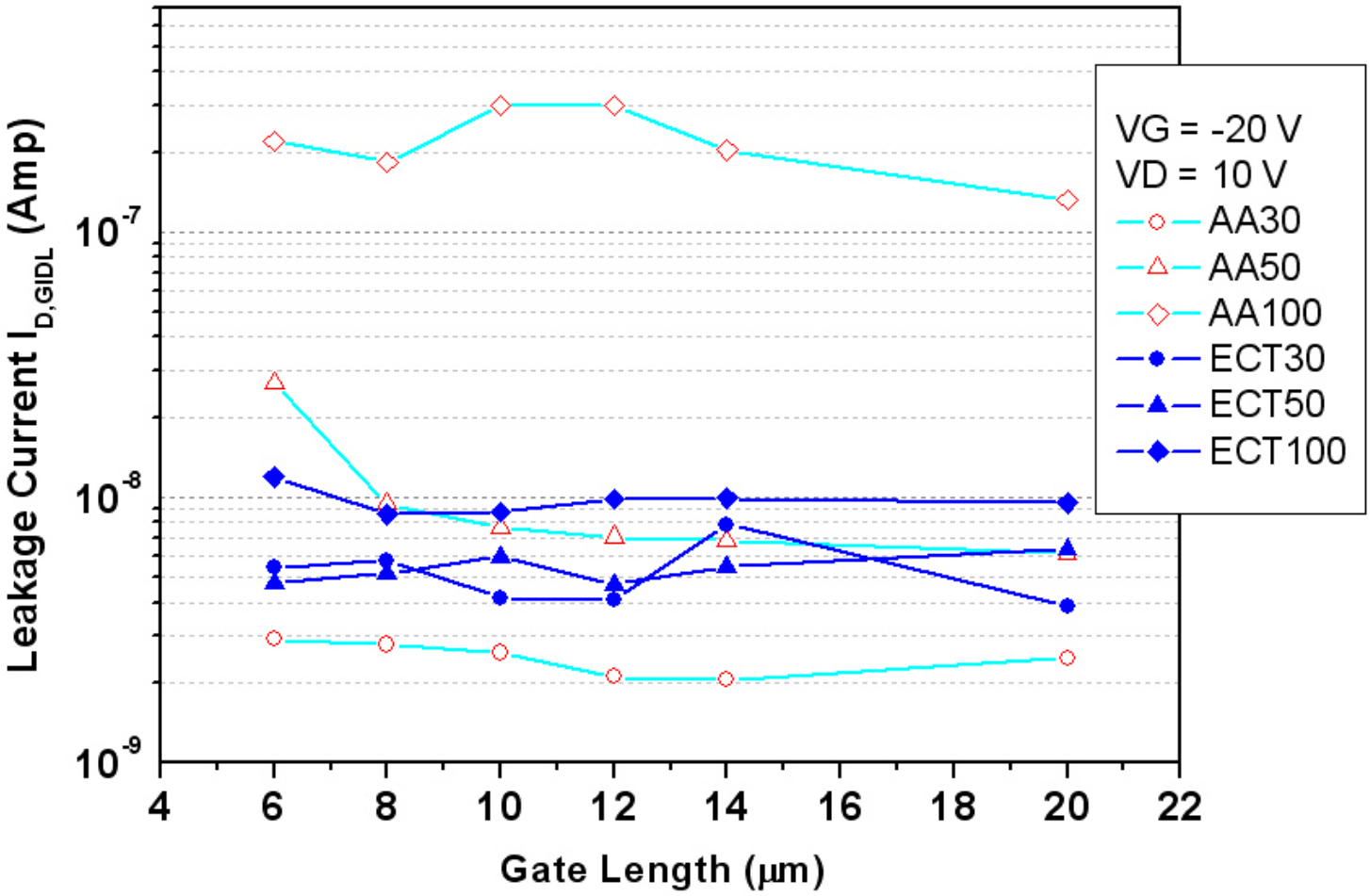

Figure 2-9 Off-state leakage current of TFTs with different channel thickness and device structure at V_G = -20 V, V_D = 10 V

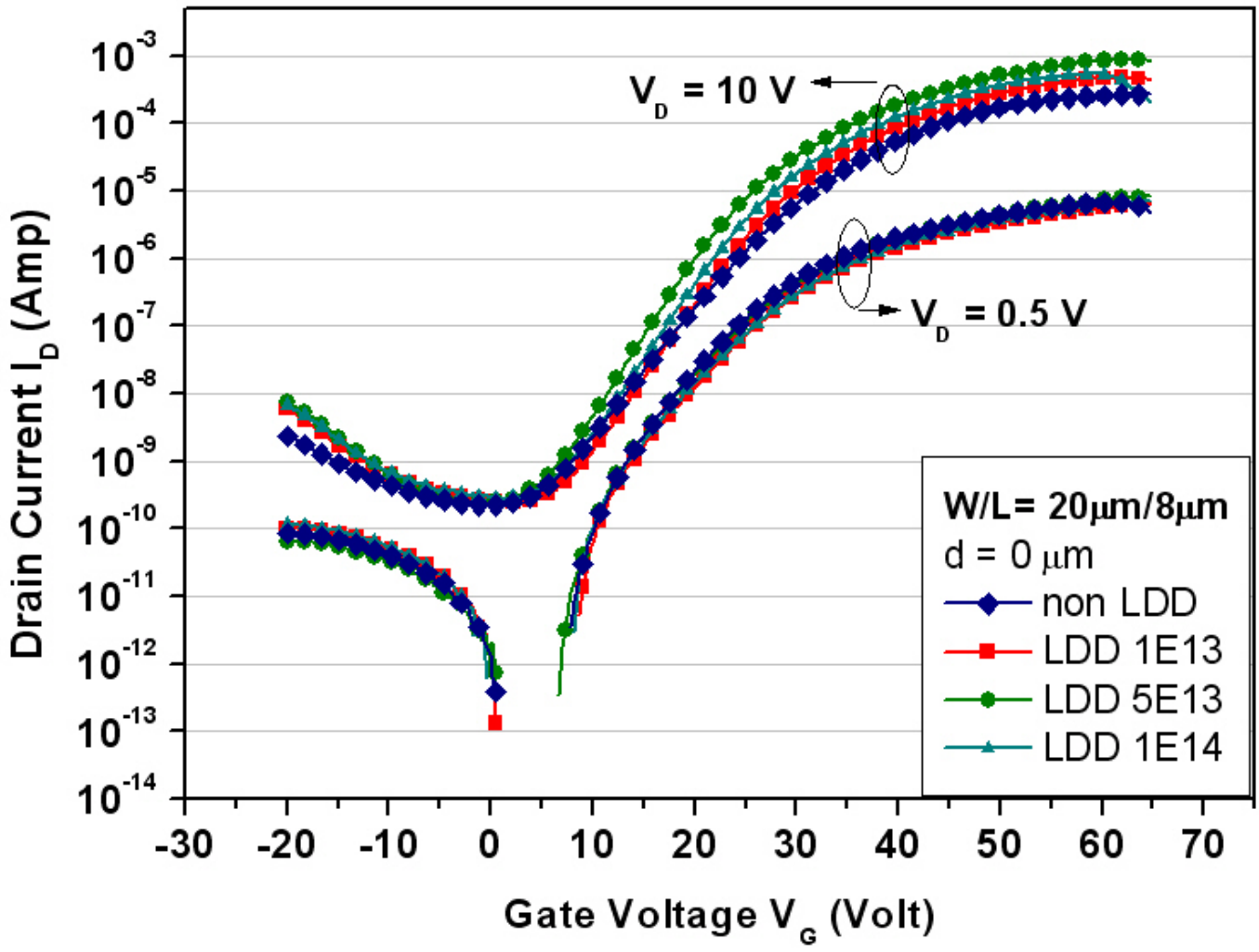

Figure 2-10 I_D - V_{GS} curves of ECTFT with various doping concentration of LDD region; W/L = 20 μm /8 μm and d = 0 μm

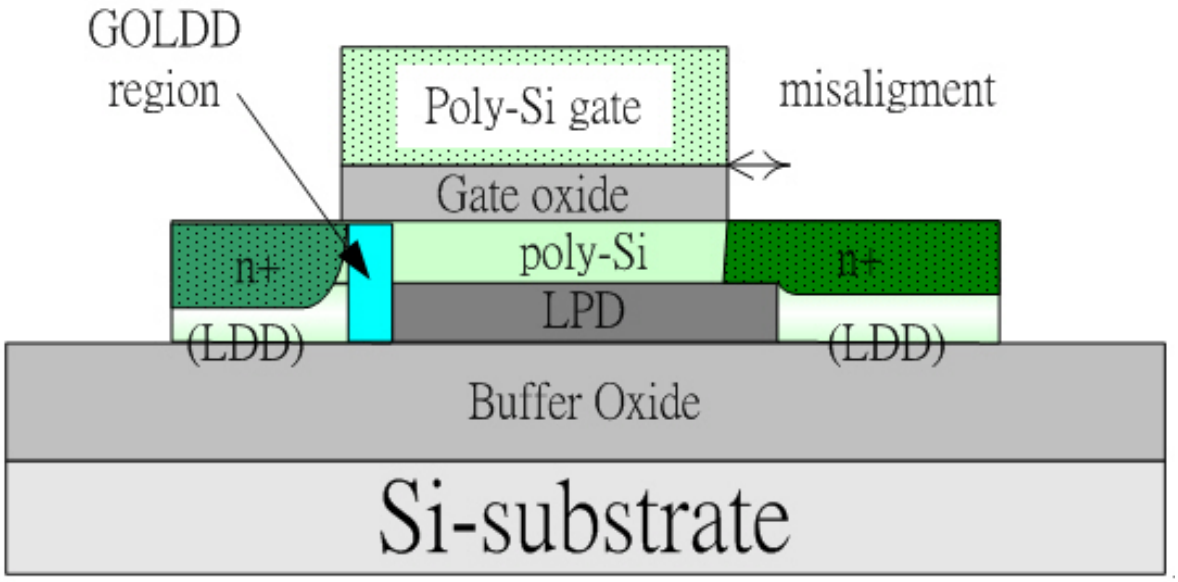

Figure 2-11 The schematic diagram for illustrating a misaligned ECTFT device with overlapped length d = 0 μm

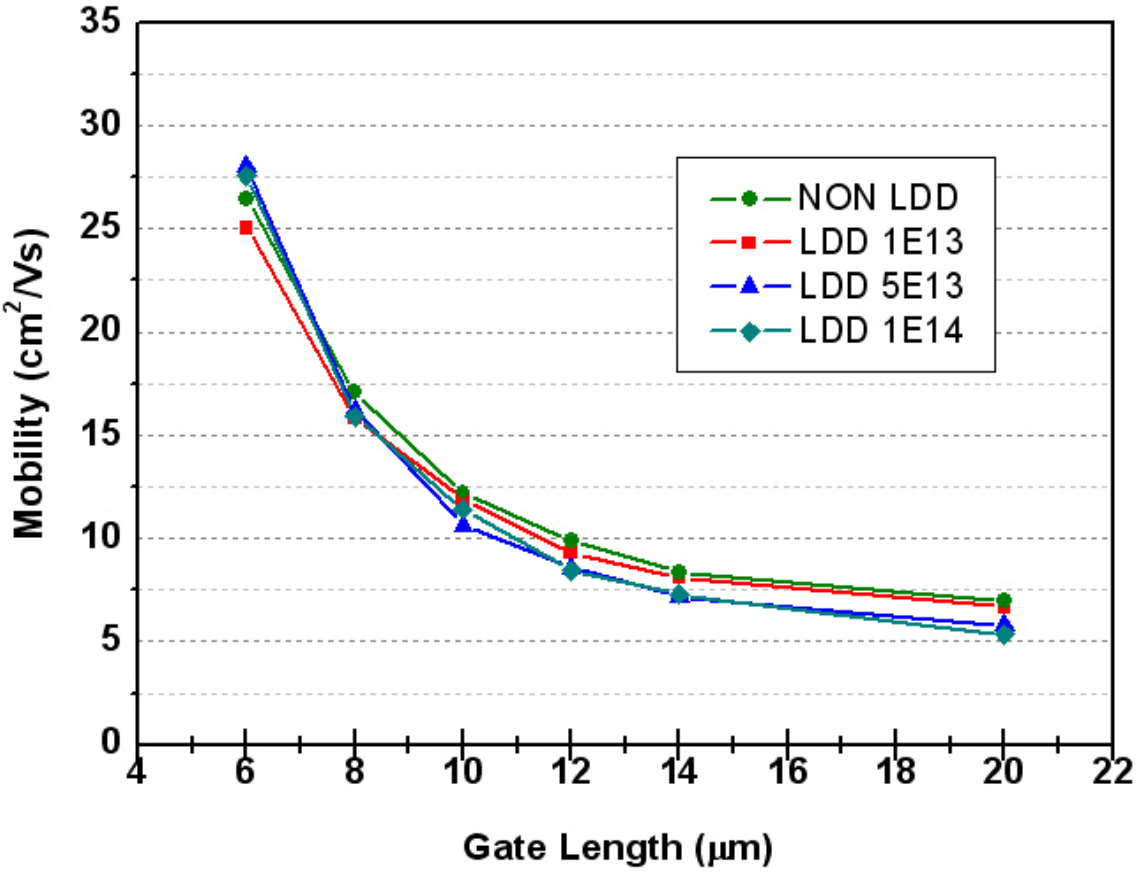

Figure 2-12 Comparison of mobility and versus gate length for ECTFT with different LDD doping concentration

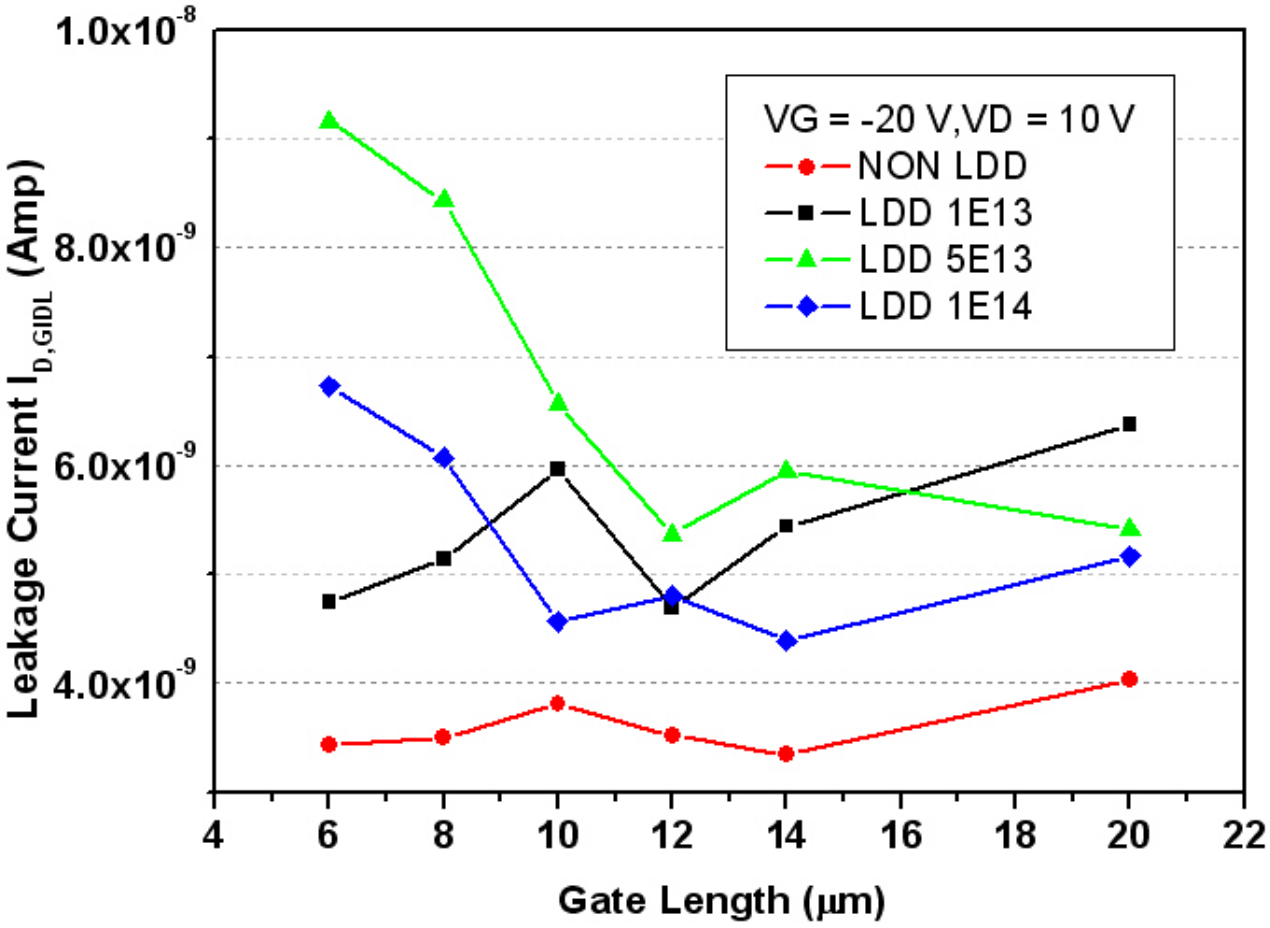

Figure 2-13 Comparison of GIDL leakage current versus gate length for ECTFT with different LDD doping concentration

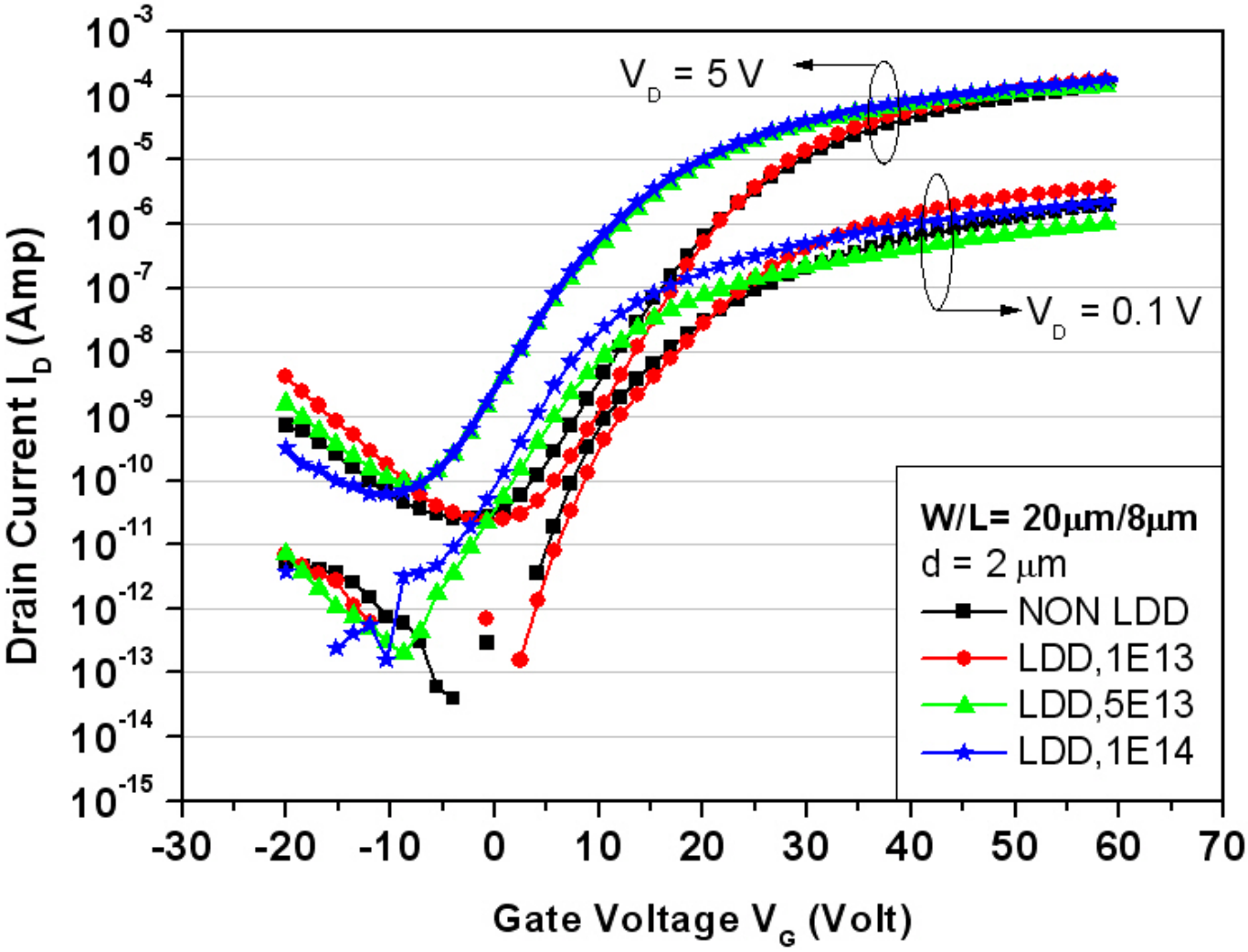

Figure 2-14 I_D - V_{GS} curves of ECTFT with various doping concentration of LDD region; W/L = 20 μm /8 μm and d = 2 μm

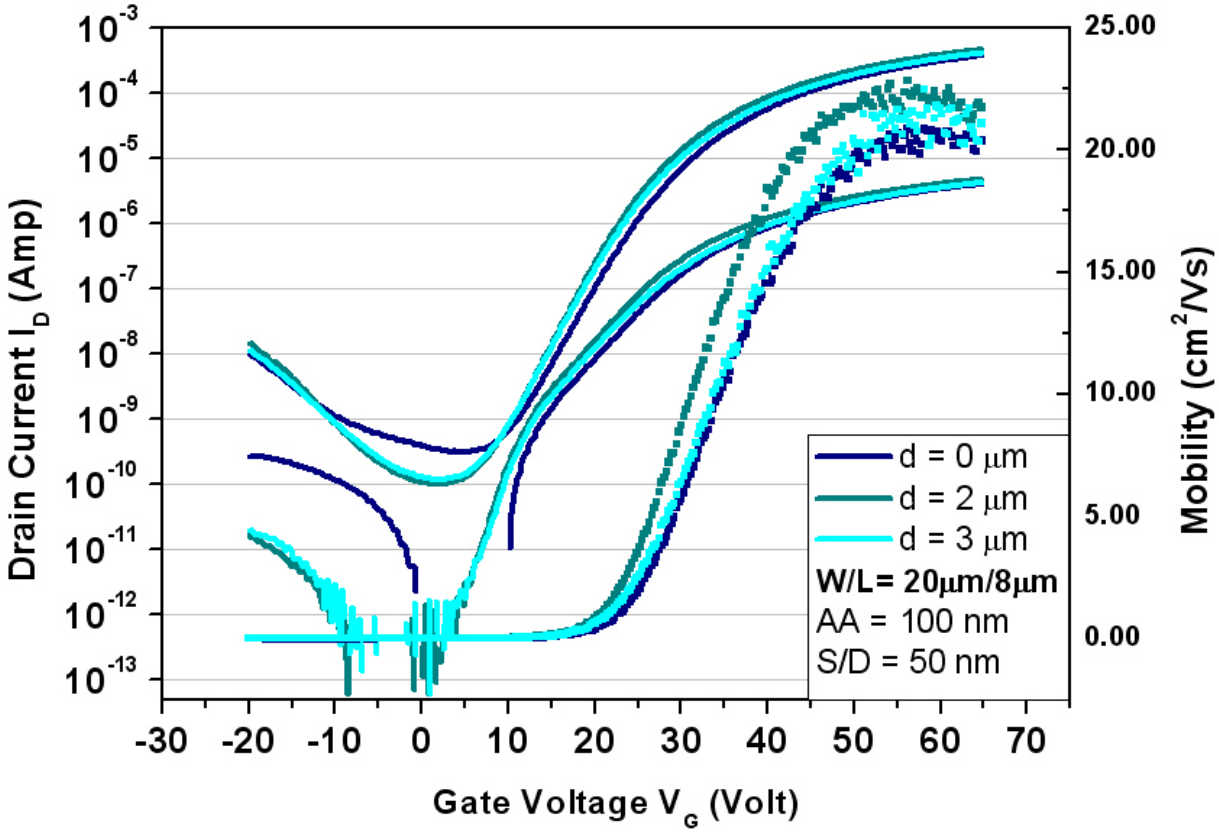

Figure 2-15 Transfer curves of ECTFT with different gate overlapped length *d*

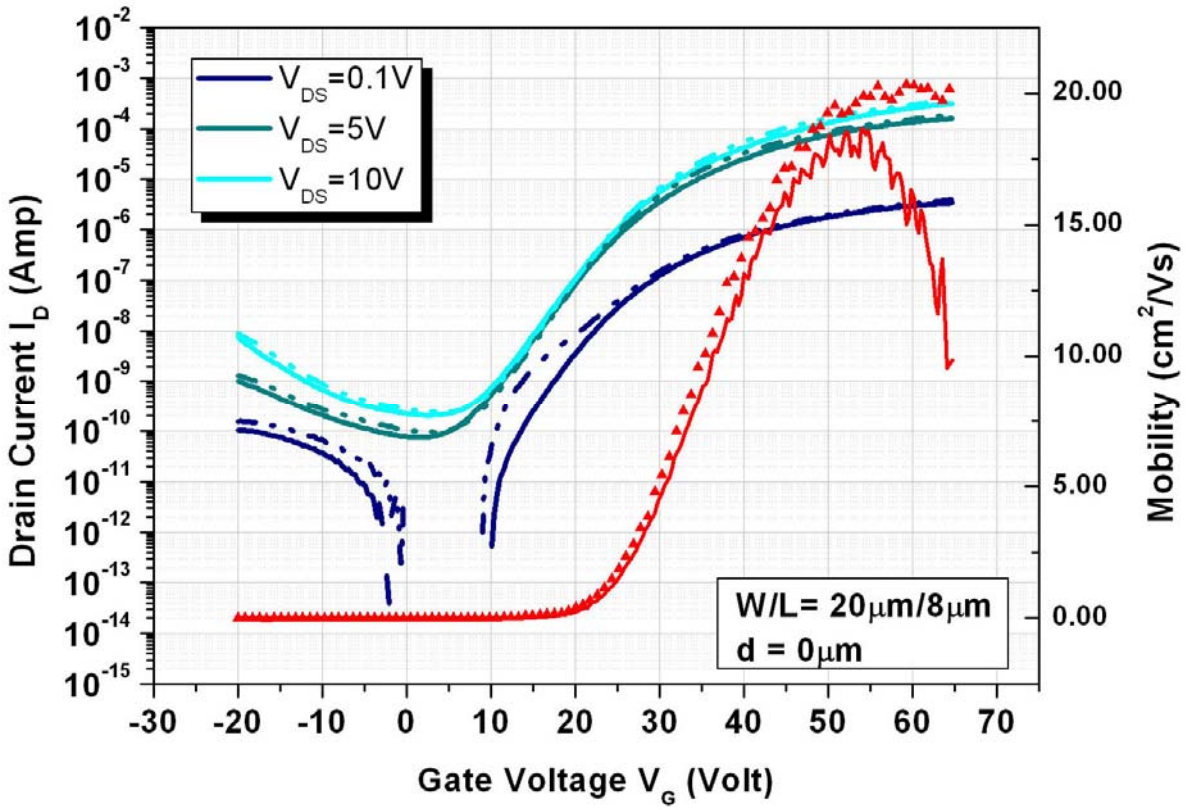

Figure 2-16 Forward (solid line) and reverse (dash line) measurement of the transfer curves of an ECTFT with W/L = 20 μm/8 μm and d = 0

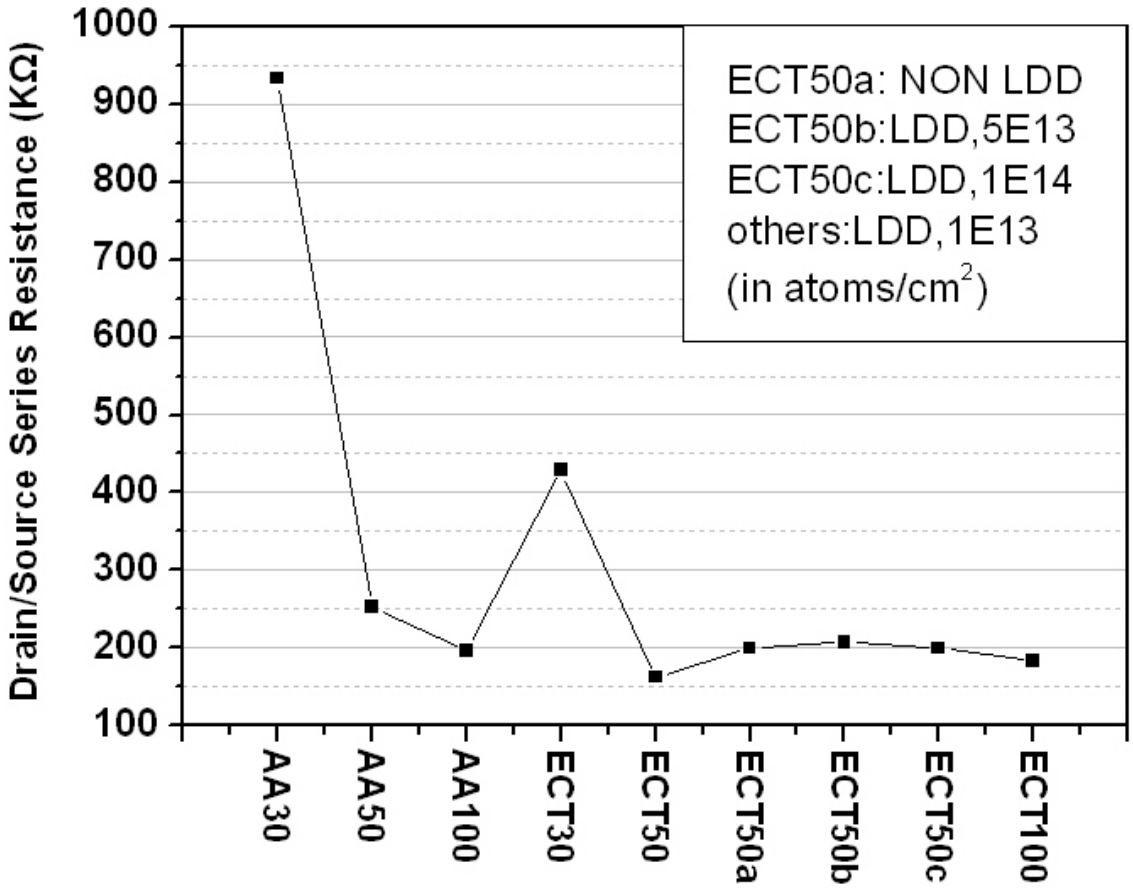

Figure 2-17 The values of the extracted source/drain series resistances for different conventional TFT and ECTFT samples

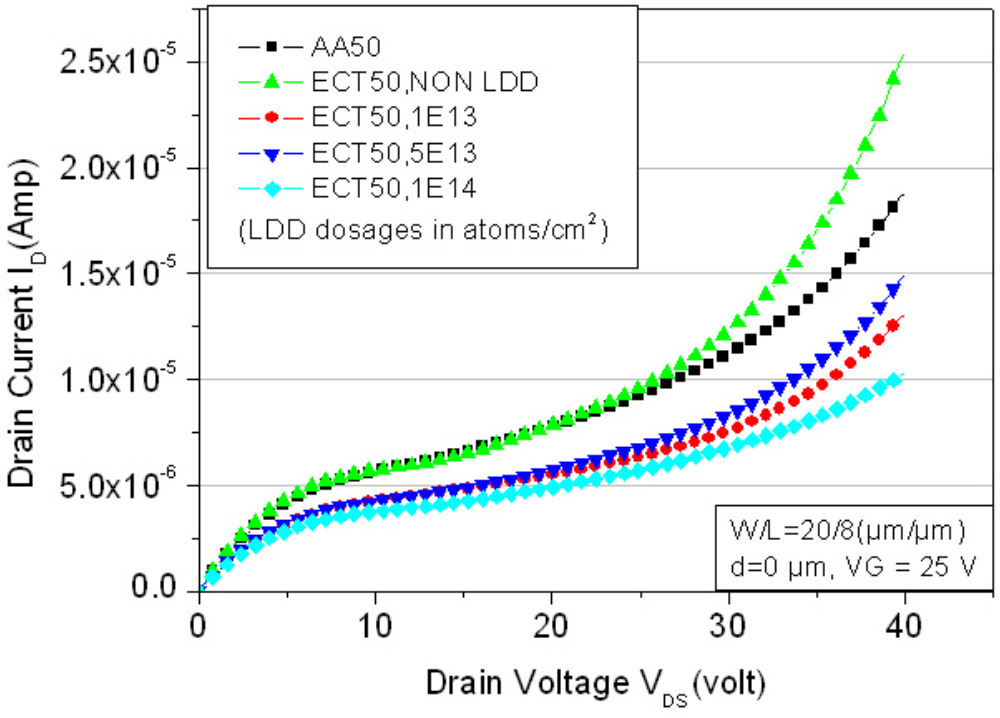

(a)

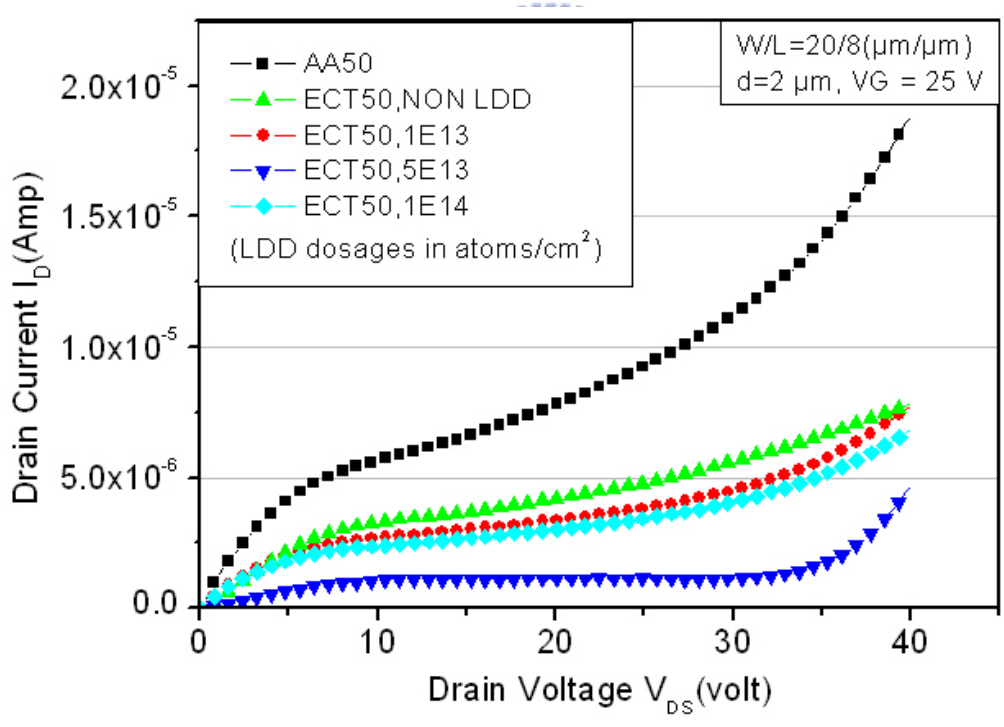

(b)

Figure 2-18 I_D - V_D curves extracted at V_G = 25 V for various TFT samples: (a) W/L = 20/8, d = 0 μm, and (b) W/L = 20/8, d = 2 μm

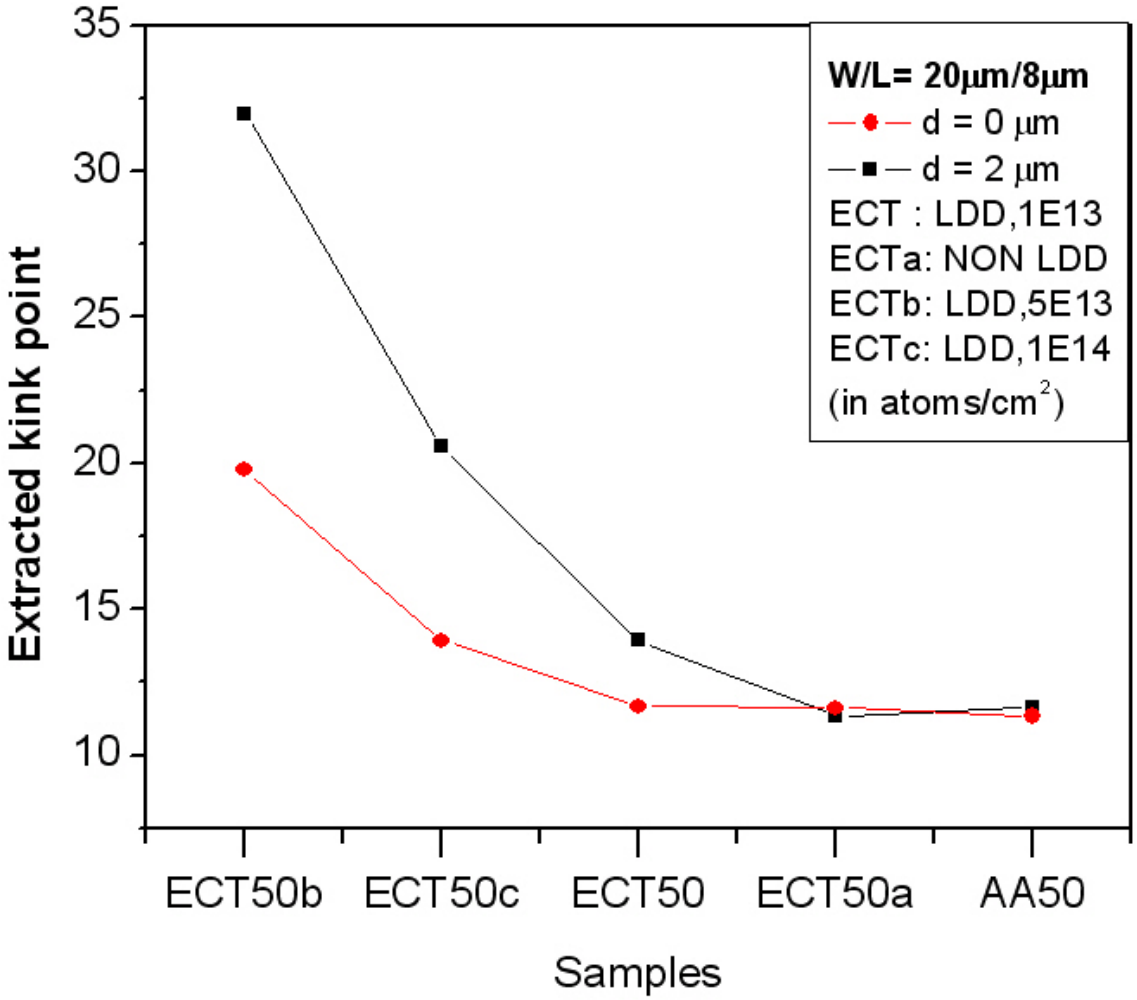

Figure 2-19 Extracted kink point for different TFT samples; W/L = 20/8 and d = 0 µm, d= 2µm